New insights into the Triangulum Australis supercluster of galaxies

Hernán Quintana, Dominique Proust, Ivan Lacerna, Hans Böhringer

A&A 667, A66 (2022)
https://doi.org/10.1051/0004-6361/202244714

Astronomy & Astrophysics

New insights into the Triangulum Australis supercluster of galaxies*

Hernán Quintana[1], Dominique Proust[2], Ivan Lacerna[3,4], and Hans Böhringer[5]

[1] Instituto de Astrofísica, Facultad de Física, Pontificia Universidad Católica de Chile, Casilla 306, Santiago 22, Chile
e-mail: hquintana@astro.puc.cl
[2] GEPI – Observatoire de Paris, 92195 Meudon Principal Cedex, France
e-mail: dominique.proust@obspm.fr
[3] Instituto de Astronomía y Ciencias Planetarias, Universidad de Atacama, Copayapu 485, Copiapó, Chile
e-mail: ivan.lacerna@uda.cl
[4] Millennium Institute of Astrophysics, Nuncio Monsenor Sotero Sanz 100, Of. 104, Providencia, Santiago, Chile
[5] Max Planck Institüt für Extraterrestrische Physik, Giessenbach Strasse 1, 85748 Garching, Germany

Received 8 August 2022 / Accepted 15 September 2022

ABSTRACT

The Triangulum Australis cluster is one of about a dozen nearby massive cluster systems which contribute to the gravitational pull behind the so-called Great Attractor that is dominated by the nearby Shapley Supercluster mass, which conforms the galaxy velocity flows observed in that general direction. Here, we study the structure and dynamical mass of the Triangulum Australis cluster together with the neighbouring cluster AS0794. We present a set of 131 velocities collected in the regions of the two clusters with the 2.5 m Du Pont telescope at Las Campanas Observatory (Chile). For the Triangulum Australis cluster we find a dynamical mass of about $M_v = 4.2\ (\pm 1.3) \times 10^{15}\ M_\odot$ and for AS0794 a value of about $M_v = 1.7\ (\pm 1.3) \times 10^{13}\ M_\odot$. These values are consistent with the observed X-ray luminosities of these clusters. Combined with velocities already known we reanalyse the structure and dynamics of this general region, finding that both clusters, together with at least eight other ones, form a large supercluster, centered on TriAus (which dominates in terms of mass). We find that this supercluster is part of a large-scale structure filament linked to the Shapley supercluster (SSC). Uncertainties remain on the richness and detailed structure of this filament and the TriAus supercluster because parts of it remain hidden behind the Galaxy disk.

Key words. galaxies: clusters: general – galaxies: distances and redshifts

1. Introduction

Redshift surveys of clusters of galaxies are needed to study their dynamical and evolutionary state. In clusters, the mean redshift is a key ingredient in deriving distances, allowing for the study of matter distribution on very large scales. Analyses of the velocity distribution within clusters can lead to an estimate of the virial mass, thus helping to constrain models of the dark matter content. Dynamical mass estimates complement measurements at other wavelengths, in particular, those obtained through X-ray observations of clusters. Discrepancies sometimes found between optical, spectroscopic and X-ray masses often point to substantial substructures in the cluster systems (e.g., Girardi et al. 1998; Cypriano et al. 2005). Virial mass estimates rely on the assumption of dynamical equilibrium.

In this paper, we build upon previous studies of the dynamical status of the Triangulum Australis (TriAus) complex cluster of galaxies with the addition of a new set of velocities obtained for the two clusters, Triangulum Australis itself and AS0794, with the Du Pont 2.50 m telescope at Las Campanas observatory (Chile). The TriAus cluster at RA = 16h38m18.2s Dec = −64°21′37″ J2000 (DSS position of the brightest cluster galaxy, BCG) is a relatively nearby (z = 0.051) bright, hot system which was overlooked in the optical band surveys due to its low galactic latitude. From the ROSAT survey, the X-ray halo has been largely investigated, centered on the BCG (Ajello et al. 2009). Figure 1 shows the X-ray contours of the TriAus from an *XMM-Newton* observation. It is the 11th X-ray brightest cluster to contribute to the illustration of how important the cluster is in terms of gravitational pull (since X-ray luminosity flags mass). The X-ray peak is a bit diffuse inside a radius about 6 arcsec and its centering is slightly off from the BCG, with an X-ray centre at RA = 16h38m21.8s, Dec = −64°21′30″ J2000.

The TriAus cluster is part of a larger structure, connected to the Ara cluster at $z \simeq 0.05$ (RA = 16h53m02.4s Dec = −59°42′59″ J2000) and separated by only ≃13.7 h^{-1} Mpc (Woudt et al. 1999; Radburn-Smith et al. 2006). There are other clusters nearby, suggesting the presence of a larger supercluster, with an extension that can continue behind the Milky Way disc. Moreover, since it is in the general direction of the "Great Attractor", at nearly the same radial recessional velocity as the Shapley supercluster (SSC, Proust et al. 2006; Quintana et al. 2020), it can play a part in "causing" the cosmic flow to that direction. Also, and more generally, it is located in the overall direction of the microwave anisotropy dipole.

The TriAus large structure is also of great interest since all its components are close to the Zone of Avoidance (ZoA), in the direction of the famous "Great Attractor" and its physical properties (redshift dispersion, mass, substructures, etc.) have not been studied in depth until now, due to their low

* Based on observations made with the 2.50 m Du Pont Telescope at the Las Campanas Observatory (Chile).

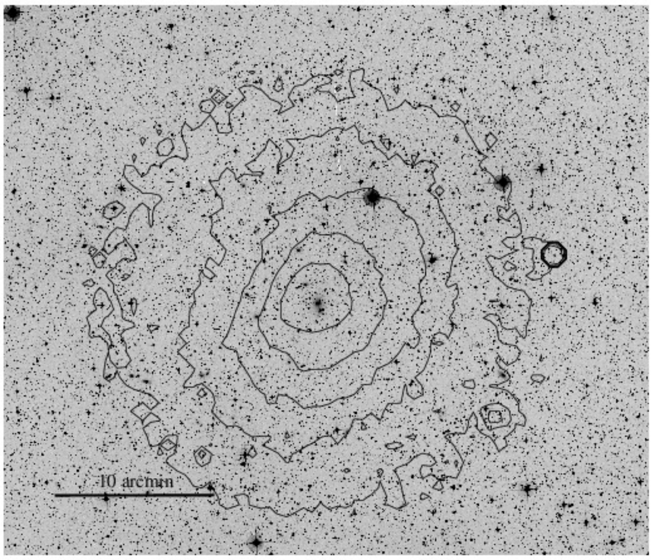

Fig. 1. X-ray contours of the Triangulum Australis cluster from an observation with *XMM-Newton* overlaid on a Digital Sky Survey image.

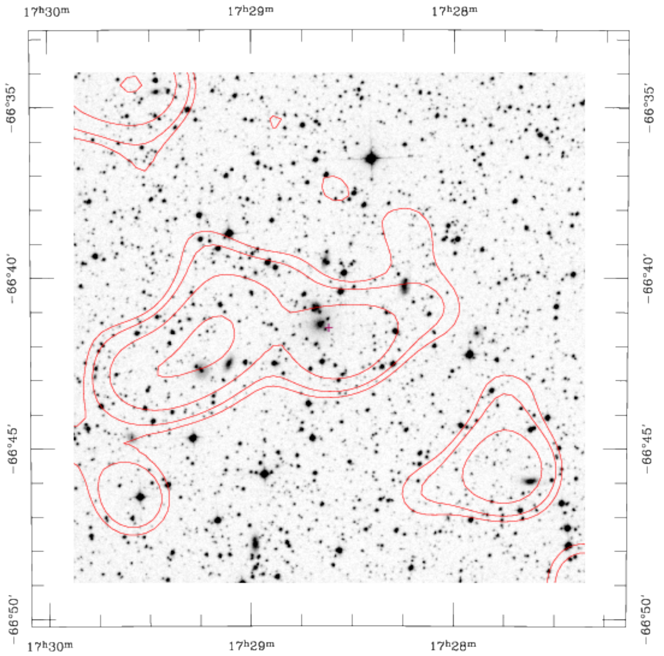

Fig. 2. X-ray contours of AS0794 from the ROSAT survey overlaid on a Digital Sky Survey image.

galactic latitude. The first target observed is an area of galaxies, which we temporarily dubbed the "C101 cluster" (for its ESO Survey field number), centered approximately at RA = 16h38mn Dec = −64°31′ (J2000), which turned to be the TriAus cluster. This target was first optically noticed by us in a serendipitous way based on a CCD small frame of a stellar field taken by one of our team for a colleague. We noticed the unusual number of galaxies for its galactic latitude and we decided to carry out further spectroscopic observations, using the end of allocated nights to observe the Shapley Supercluster, when this main target was too low in the night sky. Later it was pointed to us (Raychaudhury, priv. comm.) that an X-ray source (McHardy et al. 1981), named as 3A1633-644 had been detected, which had been extended and obviously identified with the same optical cluster. It has been observed later with the X-ray satellite ASCA (11.3 and 6.7 ks, Markevitch et al. 1996) and it was found to be a cluster with a hot (12 keV) core at its centre that was most likely produced by a merger. The cluster is close enough (5 arcmin ≃ 300 kpc) so that even at low resolution, a radio halo could be resolved. As part of the development of MeerKAT (Booth et al. 2009), a scientific test array, the Karoo Array Telescope (KAT-7), has been constructed and commissioned at the same site. A high significance diffuse radio emission was discovered in the area of TriAus with the KAT-7 array (Scaife et al. 2015), showing the potential of the array to image extended objects of low surface brightness. These authors compared the radio power from this proposed halo with X-ray and Sunyaev–Zel'dovich (SZ) measurements and demonstrates that it is consistent with the established scaling relations for cluster radio haloes.

The second target is the richness class 0 cluster AS0794 (RA = 17h28mn37.0s Dec = −66°41′28″ J2000) which has been poorly studied (Ayral & Saurer 2005). However, with a diameter of 6 arcmin and a mean redshift $z = 0.0426$, this cluster is of importance as it is situated along a filament connecting several clusters, such as AS0797 ($z = 0.0482$), CGJ1720−67.8 ($z = 0.045$), CIZA J1638.2−64.20 ($z = 0.0508$), CIZA J1645.4−73.34 ($z = 0.061$), and CIZA J1653.0−59.43 ($z = 0.048$), to the main TriAus supercluster (Chow-Martinez et al. 2014). The X-ray contours from the ROSAT survey show a faint trace of X-ray emission of about 3 photons (above a very low background) with a resulting luminosity of about 10^{42} erg s^{-1}, which is the typical luminosity of a massive single elliptical or a galaxy group (Kim & Fabbiano 2013). However this emission may be real given the fact that source photons are detected around the two bright galaxies of the cluster, as shown in Fig. 2. We note that no preferred alignment has been noted, as AS0794 and TriAus show isotropy in both their polar and azimuthal angle distributions (Ayral & Saurer 2005).

We collected a new set of velocity data in the direction of these two targets, useful for completing the existing collection of data available in the literature. In this paper, we analyze these two galaxy structures from their spectroscopic properties and we discuss the evolutionary state of the TriAus complex supercluster. In Sect. 2, we present the observations and data reduction. Section 3 contains the results as well as a dynamical analysis of the two clusters, aimed at studying the velocity dispersion in each cluster centre, as well as its variations with the radius until the measured limit of the shear up to 8 arcmin (equivalent to a radius of 0.5 h_{70}^{-1} Mpc at the cluster redshift). In Sect. 4, we analyze the TriAus supercluster as a whole. We adopt, whenever necessary, $H_0 = 70\,h_{70}$ km s^{-1} Mpc^{-1}, $\Omega_M = 0.3$, and $\Omega_\Lambda = 0.7$.

2. Observations and data reduction

The spectroscopic observations were carried out first using the fiber spectrograph and then the WFCCD, both mounted on the 2.50 m du Pont telescope at Las Campanas Observatory (LCO), Chile (Bowen & Vaughan 1973)[1]. The multifiber system first used at LCO consists of a plug plate at the focal plane, with 128 fibers running to a spectrograph coupled to the 2D-Frutti detector (Shectman 1989; Quintana et al. 2000). There were

[1] Las Campanas Observatory (LCO) is an astronomical observatory owned and operated by the Carnegie Institution for Science (CIS).

Table 1. Observing sessions and instrumentation used.

Instrument	Spectral range	Dispersion	Date
Shectograph	3500–7000	1 Å pix^{-1}	1997/03/8–10
”	”	”	1998/03/24–25
”	”	”	1998/05/22–24
”	”	”	1999/03/15–18
WFCCD	3800–7600	3.0 Å pix^{-1}	2007/02/19–23
”	”	”	2008/05/30–06/01
”	”	”	2009/03/29–04/01

105–112 fibers used for objects while 16 sky fibers were set aside, spaced at intervals of one every 6 fibers along the spectrograph entrance and positioned in a random pattern in the plug plate. Standard quartz lamp exposures of a white spot inside the dome were used to correct for pixel-to-pixel variations of the detector. The grating angle was changed to several values during these long exposures in order to properly illuminate the whole detector surface. Five-minute exposures with helium-neon and thorium-argon hollow cathode comparison lamps were taken for wavelength calibration before and after each exposure. The resulting 2D Frutti images have a 2048×1520 pixel area. The fiber images are $\simeq$8 pixels wide, separated by $\simeq$12 pixels from center to center. The exposure times were adjusted between 60 and 180 min, depending on the brightness of the galaxies and the available observing time. The WFCCD is a multislits drilled bronze mask with useful 22 arcmin × 22 arcmin field of view, taking two fields per cluster to cover central region. Blue grism 400 lines mm^{-1} was used for spectra exposure, with a 2K × 2K CCD, binned 1 × 1 with gain 1. We took 3–4900 s exposures per field and He–Ar comparison lamps taken before and immediately after each set of exposures. Table 1 summarizes the observing sessions and instrumentation used.

The data reduction was carried out at Paris observatory, Meudon campus, in order to obtain wavelength calibrated spectra then velocities. We reduced the data with the MULTIRED package (Le Fèvre et al. 1995) of IRAF[2] performing the following steps in sequence for each slit: (1) We extracted small 2D postage-stamp images corresponding to one slit from the two dimensional spectra of the object and the corresponding wavelength calibration and flat field from the full 2048×1520 pixel images. (2) We performed a flat-field correction and sky emission subtraction: the sky was fitted with adjustable low-order polynomials and subtracted along the slit for each wavelength element. A treatment of the zero-order position was also added. (3) We combined all the corrected two-dimensional spectra of a given object with average or median scheme using sigma-clipping rejection. (4) We extracted a one-dimensional spectrum of the arc-lamps and cross-correlated it with a reference arc-lamp spectrum to produce an initial wavelength solution. (5) We extracted a one-dimensional spectrum from the corrected two-dimensional spectrum for each object of interest in the slit by averaging along the wavelength axis. (6) We obtained the wavelength for the one-dimensional object spectrum and plotted the corrected and calibrated one-dimensional spectrum.

The radial velocities were determined using the cross-correlation technique (Tonry & Davis 1979) implemented in XCSAO task of the RVSAO package (Kurtz et al. 1991; Mink et al. 1995), with the spectra of radial velocity standards of late-type stars (Pickles 1998) and previously well-studied galaxies (Pickles 1985). The values of their R statistics (defined as the ratio of the correlation peak height to the amplitude of the anti-symmetric noise) are listed in Table A.1, along with the measured velocities and their formal uncertainties. For spectra with $R < 3.0$, the measured velocity was considered unreliable and was not used, except for emission-line objects where the velocity was obtained using the EMSAO task implemented in the RVSAO package.

[2] IRAF is distributed by the National Optical Astronomy Observatories, which are operated by the Association of Universities for Research in Astronomy, Inc., under cooperative agreement with the National Science Foundation.

Table 2. Identified clusters of galaxies in the same region with velocities between 8000 and 20 000 km s^{-1}.

(1)	(2)	(3)	(4)	(5)
Abell S0727	MCXC J1320.7−4102	13 20 42.7	−41 02 22	14 839
Abell S0729		13 21 32.2	−35 47 41	14 960
Abell S0731		13 23 01.9	−34 52 39	15 140
Abell 3556		13 24 06.2	−31 39 37	14 309
Abell 3558	Shapley centre	13 27 57.5	−31 30 09	14 390
Abell S0734		13 27 55.2	−41 07 31	15 080
RXSC J1328−3233		13 28 51.8	−32 33 21	14 450
MCXC J1329.8−3310	400d J1329−3310	13 29 49.4	−33 10 23	15 319
Abell 3560	RXC J1332.3−3308	13 32 22.6	−33 08 21	14 666
Abell 3562	MCXC J1333.6−3139	13 33 36.3	−31 49 40	14 740
Abell 3564	SSGS 091	13 34 22.3	−35 13 21	15 140
Abell S0737		13 35 26.1	−40 04 19	15 174
RXS J1337.7−4120	MCXC J1337.4−4120	13 37 28.2	−41 20 00	15 559
Abell 3566	SSGC096	13 38 59.4	−35 33 12	15 469
Abell 3568		13 41 11.1	−34 38 08	15 483
Abell S0739		13 42 53.7	−34 58 05	15 318
Abell S0740		13 43 32.3	−38 11 04	10 073
Abell S0742		13 44 35.5	−34 18 02	15 277
Abell S0743		13 46 16.3	−39 53 59	11 316
Abell 3570		13 46 52.5	−37 52 37	10 972
Abell 3571	SSGC 104	13 47 28.4	−32 50 58	11 700
Abell 3572		13 48 11.4	−33 22 55	15 499
RXSC J1349−3334		13 49 18.5	−33 34 37	11 662
Abell S0746		13 49 49.0	−34 58 52	14 877
Abell S0748		13 52 35.4	−32 23 46	11 866
Abell 3575	SSGC 115	13 52 35.8	−32 52 46	11 242
[*MHS* 2013] 091		13 58 15.3	−36 29 36	9773
Abell S0754		14 06 20.5	−39 49 17	9695
CIZA J1410.4−4246	MCXX J1410.4−4246	14 10 28.5	−42 46 36	14 690
Abell S0757		14 12 15.2	−33 08 03	13 191
Abell S0758		14 12 22.3	−34 19 03	11 392
Abell S0763		14 22 57.0	−31 07 37	19 429
Abell 3603		14 33 17.1	−31 48 10	18 018
Abell S0772		14 43 01.0	−42 17 43	16 118
Abell S0774		14 49 23.6	−40 21 25	18 587
CIZA J1514.6−4558	MCXC J1514−4558	15 14 35.9	−45 58 49	17 388
CIZA J1518.3−4632	MCXC J1518.3−4632	15 18 22.8	−46 32 35	16 788
CIZA J1535.1−4658	MCXC J1535.1−4658	15 35 09.1	−46 58 45	10 793
CIZA J1614.1−6307		16 14 07.9	−63 07 50	18 587
TriAus cluster	MAXI J1638−643	16 38 18.2	−64 21 37	14 992
Ara cluster	PSZ2 G329.36−0990	16 53 02.4	−59 42 59	14 390
CG J1720-67.8		17 20 28.5	−67 46 39	13 491
Abell S0794		17 28 37.0	−66 41 28	12 669
[*MHS* 2013] 126		17 40 01.6	−48 56 53	17 688
Abell S0797		17 52 24.0	−65 28 42	14 450
[*MHS* 2013] 133		18 08 25.8	−40 09 00	17 658
Abell S0801		18 27 27.4	−51 32 08	15 319
Abell S0800		18 28 14.0	−77 10 12	12 575
Abell 3632		18 39 42.9	−46 39 15	12 351
Abell S0808	PSZ G347.62−21.62	19 00 42.5	−49 05 45	14 729

2.1. X-ray data

For the study of the Triangulum Australis cluster in X-rays, we used data from an observation with *XMM-Newton* with the

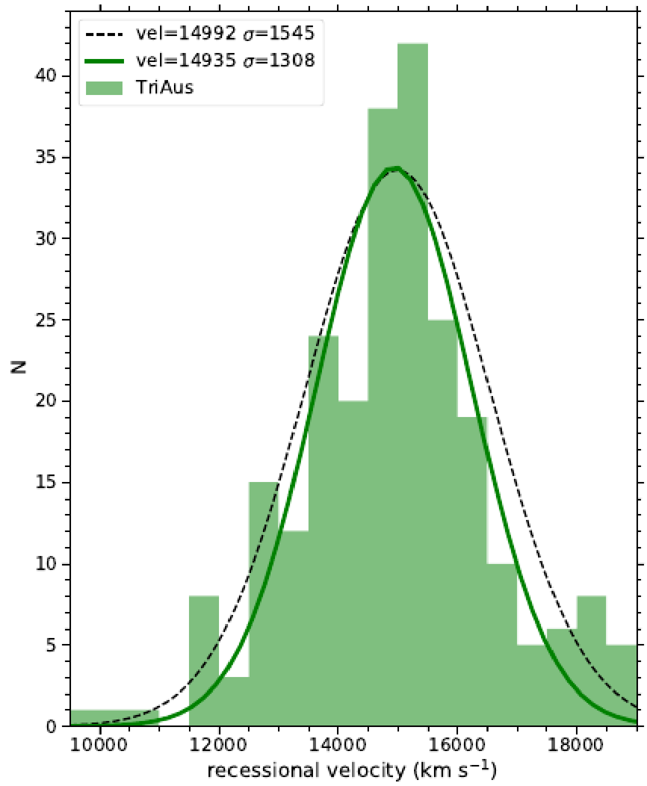

Fig. 3. Histogram of galaxy recessional velocities in the TriAus cluster with all recession velocities available in the range of $9500 \leq v \leq 19\,000\,\mathrm{km\,s^{-1}}$, with a step size of $500\,\mathrm{km\,s^{-1}}$. The lines show Gaussian distributions fitted to the data including all galaxies (dashed line) and excising the substructure of 26 galaxies (solid line).

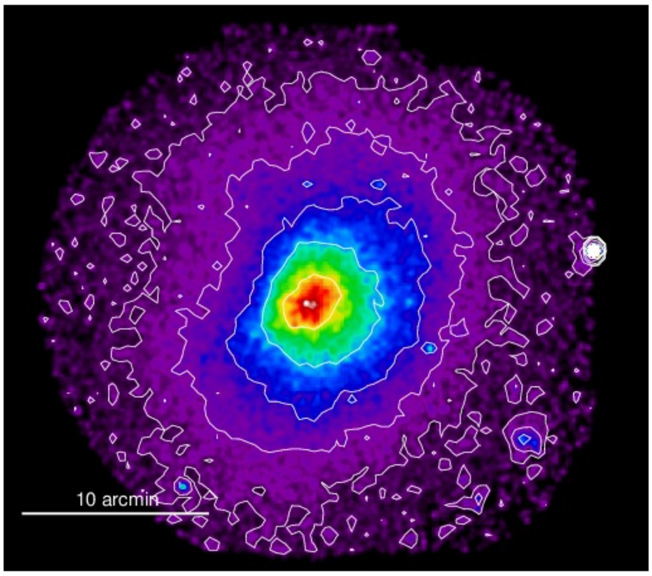

Fig. 4. *XMM-Newton* image of the Triangulum Australis cluster in the 0.5–2 keV band extending over the whole field of view (about 40 arcmin diameter).

observation ID 0093620101. The exposure time is 9, 9.8, and 3.2 ks for the MOS1, MOS2, and PN detectors respectively. The exposures have been cleaned from times affected by solar flares. For the image analysis, we focused on the 0.5–2 keV energy band, since this provides the best signal to noise ratio (S/N) above the background.

To obtain an overview on the place of the Triangulum Australis cluster in the large-scale structure environment, we use the results of the identification of galaxy clusters in the ROSAT All-Sky Survey (Trümper 1993). Clusters have been identified in a systematic, highly complete survey outside the zone of highest galactic absorption (hydrogen column density larger than $2.5 \times 10^{21}\,\mathrm{cm^{-2}}$) in the CLASSIX galaxy cluster survey (Böhringer et al. 2016), which combines the previous REFLEX and NORAS surveys (Böhringer et al. 2013, 2017). The survey reaches an X-ray flux limit of $F_X = 1.8 \times 10^{-12}\,\mathrm{erg\,s^{-1}\,cm^{-2}}$ in the 0.1–2.4 keV energy band and covers 8.25 ster of the sky. We discuss the cluster environment of the Triangulum Australis in Sect. 5.

3. Velocities catalogue

From the observing runs, we obtained a set of 131 heliocentric radial recessional velocities (some of them were observed two times) belonging to the two clusters, namely: 76 for TriAus and 55 for AS0794). Table A.1 in Appendix A lists the details of these new observations: (1) object number, (2) right ascension (J2000), (3) declination (J2000), (4) heliocentric radial recessional velocity in $\mathrm{km\,s^{-1}}$, (5) associated error in $\mathrm{km\,s^{-1}}$, (6) R value from Tonry & Davis (1979) and (7) notes.

Some galaxies have been previously observed and adding their velocities available from the NED database[3] we obtained a total of 296 velocities for TriAus and 109 for AS0794 in the range of $5000 \leq V \leq 30\,000\,\mathrm{km\,s^{-1}}$. From the linear regression to compare 43 velocities in common with the literature, we obtain $v_{\mathrm{obs}} = 0.9914 v_{\mathrm{NED}} + 62.1$, with $R^2 = 0.9978$.

4. Analyses of the clusters TriAus and AS0794

4.1. TriAus cluster

Figure 3 shows the combined distribution of 242 galaxies (76 from the present paper and 166 from NED) as wedge diagrams in RA (left) and Dec (right) of the whole velocity data until $20\,000\,\mathrm{km\,s^{-1}}$. Figure 4 shows the recession velocity distribution of these galaxies in the range of $9500 \leq v \leq 19\,000\,\mathrm{km\,s^{-1}}$, with a step size of $500\,\mathrm{km\,s^{-1}}$. The Gaussian distribution (dashed line) is centered at $14\,992\,\mathrm{km\,s^{-1}}$ with a dispersion $\sigma = 1545^{+65}_{-77}\,\mathrm{km\,s^{-1}}$. The TriAus cluster has a relatively similar average recessional velocity to the Ara cluster, both of them being physically separated by only $\simeq 13.7\,h^{-1}$ Mpc (Radburn-Smith et al. 2006) and both lying behind the Norma one, at an average recessional velocity of $v = 4707\,\mathrm{km\,s^{-1}}$.

We note that in Fig. 3, a subcomponent is visible in the range of 17 400–18 800 $\mathrm{km\,s^{-1}}$ (26 galaxies) centered at $18\,080\,\mathrm{km\,s^{-1}}$, with a dispersion of $\sigma = 617^{+65}_{-48}\,\mathrm{km\,s^{-1}}$. Markevitch et al. (1996) established the presence of substructures in the cluster. They concluded on the presence of a subcluster merger corresponding to the above subcomponent close to the centre of TriAus (see Fig. 1 of Markevitch et al. 1996). They detected a significant temperature peak in the cluster core and a temperature increase in the sector coincident with the detected subcluster. It suggests a heating of the local intracluster medium by shocks from the subcluster merger. The *XMM-Newton* data on the cluster extends

[3] The NASA/IPAC Extragalactic Database (NED) is operated by the Jet Propulsion Laboratory, California Institute of Technology, under contract with the National Aeronautics and Space Administration.

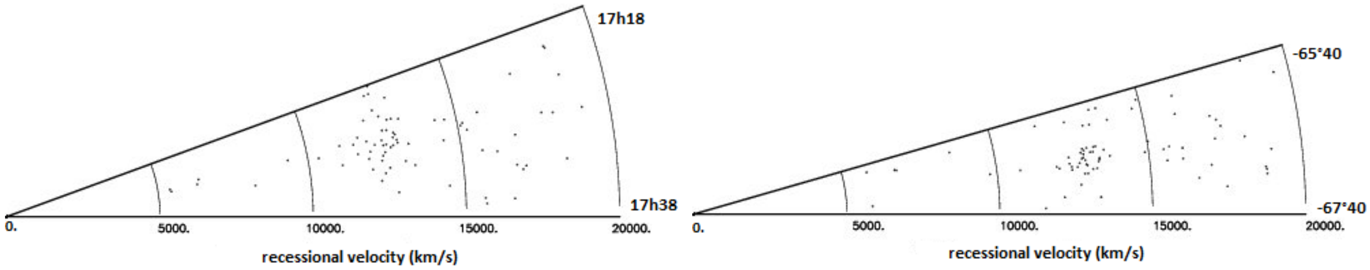

Fig. 5. Two projections in RA 17h18 to 17h38 (*left*) and Dec −65°40 to −67°40 (*right*) of galaxies of the AS0794 cluster. The angle in RA is expanded by a factor of 4 and in Dec by a factor of 8 relative to their true size for clarity.

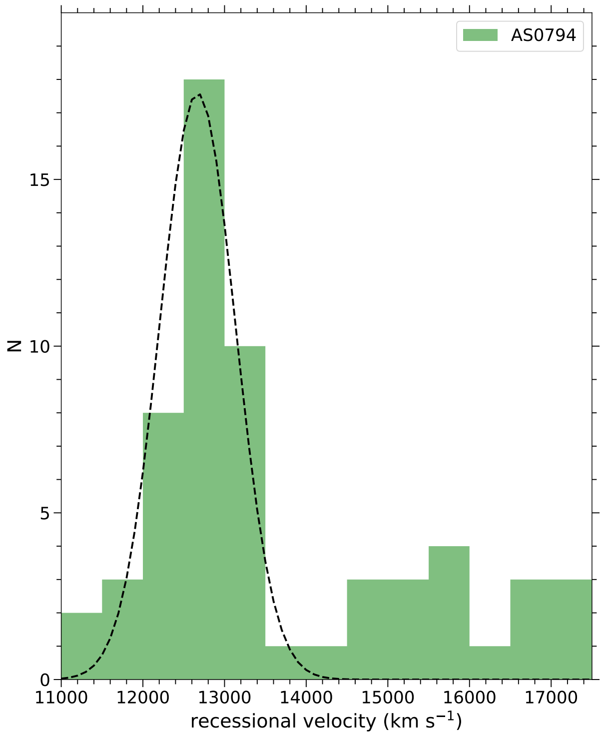

Fig. 6. Histogram of galaxy recessional velocities in the AS0794 cluster with all velocities available in the range of $11\,000 \leq v \leq 17\,500\,\mathrm{km\,s^{-1}}$, with a step size of $500\,\mathrm{km\,s^{-1}}$. The line shows a Gaussian distribution fitted to the data.

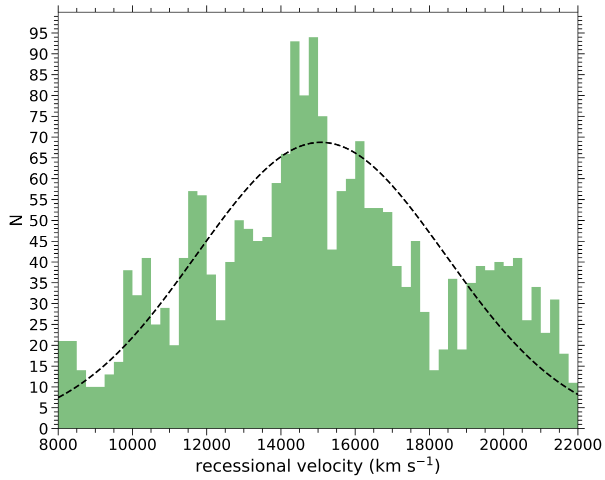

Fig. 7. Histogram of the 2328 galaxy recessional velocities in the central area 10° radius area around the Triangulum Australis cluster, with velocities available in the range of $8000 \leq v \leq 22\,000\,\mathrm{km\,s^{-1}}$ and a step size of $250\,\mathrm{km\,s^{-1}}$. The Gaussian is centered at $\overline{V} = 15\,077\,\mathrm{km\,s^{-1}}$.

over the whole field of view (about 40 arcmin diameter), displaying a quite regular cluster apart from the north-east side, which is squashed (Fig. 4): this is the side where Markevitch et al. (1996) found the higher temperature and also where the above subcomponent is situated. If we remove these 26 galaxies of the subcomponent, the Gaussian distribution on Fig. 3 (solid line) is then centered at $14\,935\,\mathrm{km\,s^{-1}}$, with a dispersion of $\sigma = 1308^{+61}_{-72}\,\mathrm{km\,s^{-1}}$.

In order to test the above conclusions, we applied the method developed by Dressler & Shectman (1988) with the δ parameter to test for kinematical structures defined as:

$$\delta^2 = (11/\sigma^2[(\overline{v}_{\mathrm{local}} - \overline{v})^2 + (\sigma_{\mathrm{local}} - \sigma)^2], \quad (1)$$

where v_{local} and σ_{local} are the local velocities and dispersions calculated from the ten nearest neighbors of each galaxy within the r_{200} radius which defines the limits of the virialized cluster from its redshift and velocity dispersion (i.e., with average density 200 times the critical one; see e.g., Diaferio et al. 2001; Finn et al. 2004):

$$r_{200} = 1.73 \frac{\sigma_{\mathrm{v,cl}}}{1000\,\mathrm{km\,s^{-1}}} \frac{1}{\sqrt{\Omega_\Lambda + \Omega_{\mathrm{o}}(1 + z_{\mathrm{cl}})^3}}\,h^{-1}\,\mathrm{Mpc}. \quad (2)$$

In random redistributions of the measured galaxy redshifts and positions, with $r_{200} \simeq 2.23\,h^{-1}\,\mathrm{Mpc}$ (37.31 arcmin), we found the sum of the δ values to be equal to or larger than the observed value with a frequency of $P_\delta = 0.224$. This value is marginally significant to conclusively verify the existence of substantial substructures. If we remove the 26 galaxies of the putative subcluster, then we have an almost perfect Gaussian velocity distribution.

The virial mass estimate of this TriAus cluster member can be computed from the 3D intrinsic velocity dispersion σ_{v} within r_{200} (Biviano et al. 2006) with:

$$M_{\mathrm{v}} \equiv (1.5 \pm 0.02)\left(\frac{\sigma_{\mathrm{v}}}{10^3\,\mathrm{km\,s^{-1}}}\right)^3 \times 10^{14}\,M_\odot\,h^{-1} \quad (3)$$

The intrinsic velocity dispersion σ_{v} is corrected from the velocity dispersion profile following Fig. 4 of Biviano et al. (2006), which gives for TriAus $M_{\mathrm{v}} = (4.2 \pm 0.7 \pm 0.6) \times 10^{15}\,M_\odot$. Here, the first error is statistical and the second one reflects the theoretical uncertainty on the relation (Sereno et al. 2010). Radburn-Smith et al. (2006) obtained a mass: $M_{\mathrm{v}} = 5.7 \pm 0.6 \times 10^{15}\,h^{-1}\,M_\odot$. If we remove the 26 galaxies from the substructure, then we obtain for TriAus a mass of $M_v = (3.2 \pm 0.6 \pm 0.5) \times 10^{15}\,M_\odot$.

For the X-ray luminosity of TriAus measured in the ROSAT survey, we obtained a value of $L_X = 6.2 \times 10^{44}$ erg s^{-1} (0.1–2.4 keV), which would imply a mass around $10^{15}\,M_\odot$ based on the X-ray luminosity mass relation (e.g., Böhringer et al. 2013, 2017), which is lower than the dynamical mass. The X-ray luminosity found by Markevitch et al. 1996 is 6.8×10^{44} erg s^{-1}, consistent with our result if converted to the 0.1–2.4 keV band and $h_{70} = 1$. From the mass–X-ray temperature relation (e.g., Arnaud et al. 2005) and the derived dynamical mass, we would expect a temperature around 13 keV, which is a bit higher than the peak temperature found by Markevitch et al. (1996). The expected X-ray luminosity for the quoted dynamical mass would be about 3×10^{45} erg s^{-1} (0.1–2.4 keV), while for an intracluster medium temperature of 10–12 keV, the expected luminosity would be about $1.3{-}2 \times 10^{45}$ erg s^{-1} (0.1–2.4 keV); this is higher by a significant factor than what is observed (using e.g., relations by Pratt et al. 2009). There is thus a clear departure of the cluster from the general scaling relations, which is certainly a sign of a non-relaxed state. This is also indicated by the squashed appearance of the cluster on the north-eastern side and the disturbed central surface brightness of the cluster which is less peaked than typically found in relaxed clusters. We therefore expect that the velocity dispersion and the cluster temperature is increased due to the distortion in comparison to a relaxed cluster of same mass, while the X-ray luminosity is reduced due to a less dense core.

Radburn-Smith et al. (2006) also computed for the Ara cluster (with a bimodal velocity distribution) a mass of $(2.0 \pm 0.3) \times 10^{15}\,h^{-1}\,M_\odot$. Considering their respective masses, it has a sizeable influence on the X-ray based dipole (Kocevski et al. 2004). As pointed out by Radburn-Smith et al. (2006), both clusters have the same velocity than the SSC (Proust et al. 2006; Quintana et al. 2020) and form an extension of the SSC in association with the two clusters CIZA J1410.4−4246 and CIZA J1514.6−4558.

4.2. AS0794 cluster

Figure 5 shows the combined resulting distribution of 78 galaxies (55 from the present paper and 23 from NED) in the AS0794 cluster as wedge diagrams in right ascension and declination of the whole velocity data available until 20 000 km s^{-1}. Figure 6 shows the recession velocity histogram of these galaxies in the range of $11\,000 \leq v \leq 17\,500$ km s^{-1}, with a step size of 500 km s^{-1}. The histogram shows the Gaussian distribution centered at 12 669 km s^{-1} with a dispersion $\sigma = 464^{+72}_{-70}$ km s^{-1}. We see on these two diagrams that there are galaxies with higher velocities than the cluster, spread towards and around the average velocity ($\simeq$15 000 km s^{-1}) of the TriAus cluster. We can suggest that AS0794 is slightly in front of the main structure linked to the TriAus complex, as dicussed below. From these velocity values and following the same procedure as for TriAus, for the cluster AS0794, we deduced $M_v = (1.7 \pm 0.7 \pm 0.6) \times 10^{13}\,M_\odot$. With this mass, we would expect an X-ray luminosity around $L_X \sim 10^{42}$ erg s^{-1}, which agrees with our observation of the cluster in the ROSAT survey.

5. Triangulum Australis complex as a part of a larger superstructure

The TriAus cluster appears to be associated with other clusters in its vicinity. Four clusters were already identified by (Kocevski & Ebeling 2006; Radburn-Smith et al. 2006) as part of a possible extension from the Shapley Supercluster (SSC) in the SE direction: the TriAus cluster, the Ara cluster, CIZA J1410.4−4246, and CIZA J1514.6−4558. In fact, Radburn-Smith et al. (2006) remarked that A 3558 (at the core of the SSC) lies only 38 Mpc from CIZA J1410.4−4246, so that the TriAus complex can form an extension of the SSC (at the same average velocity). For Kocevski & Ebeling (2006), this web of

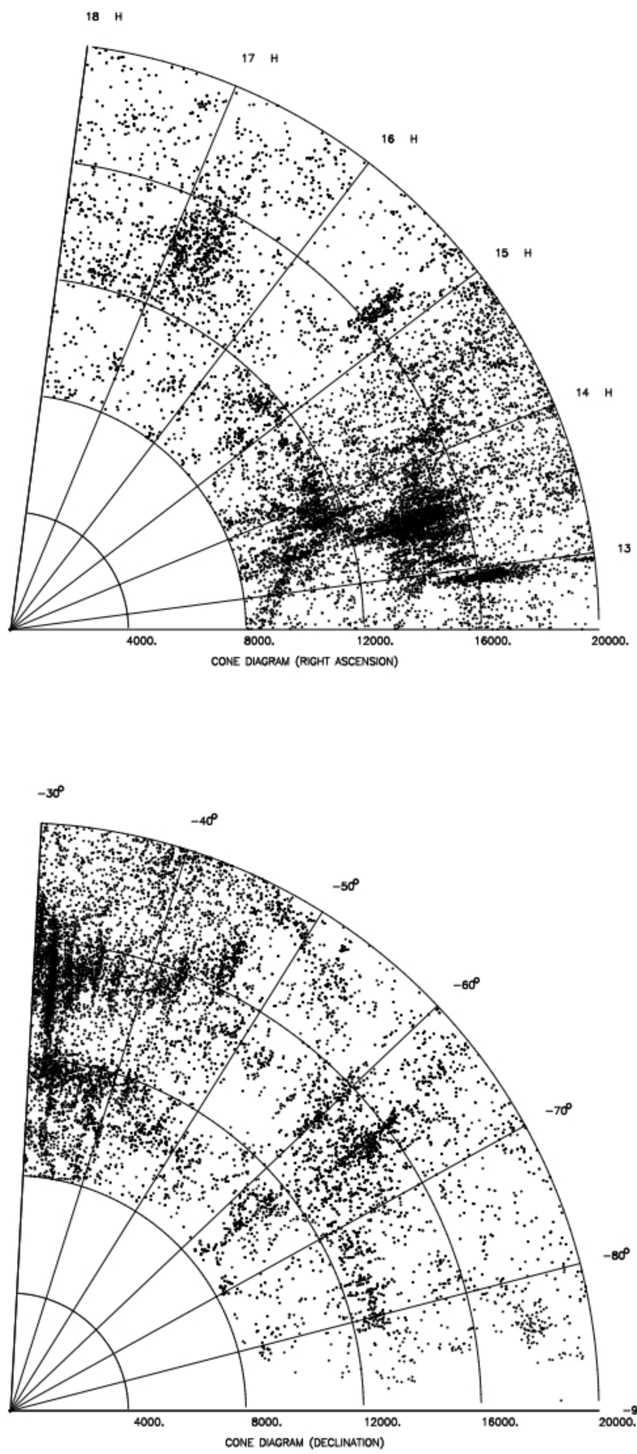

Fig. 8. Wedge diagram in RA and Dec of the complete region between the Triangulum Australis and the Shapley clusters from RA = 12h30 to RA = 18h and from Dec = −30° to Dec = −90°. The Dec diagram is enlarged by a factor of 1.5 for clarity.

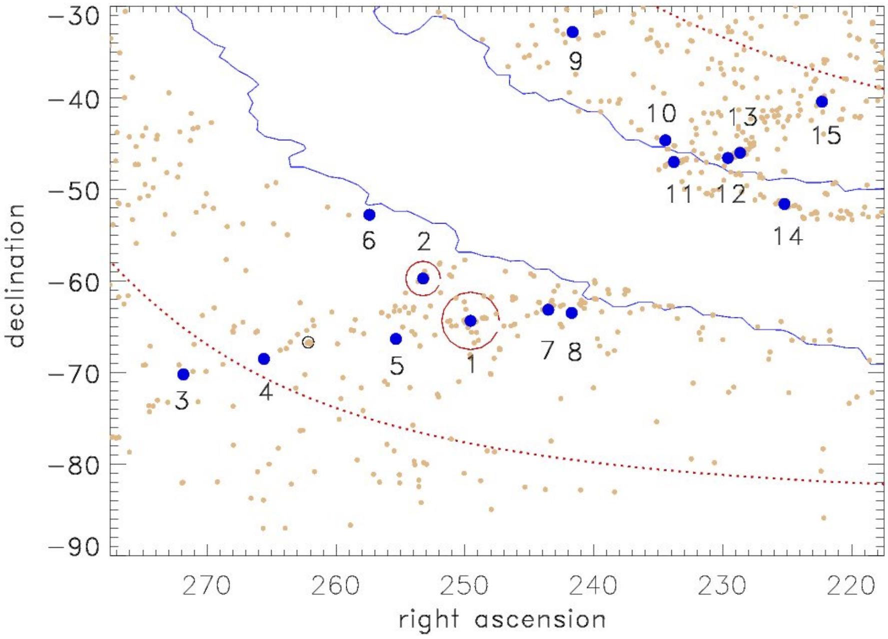

Fig. 9. Selection of 15 X-ray luminous CLASSIX clusters and 2MASS galaxies (0.003 < z < 0.065) in the Triangulum Australis region, with the high galactic absorption region inside the two blue lines. Triangulum Australis cluster is marked by a larger red circle and the Ara one by a smaller red circle. AS0794 is marked with an open circle and the number for the other clusters are given in Table 3.

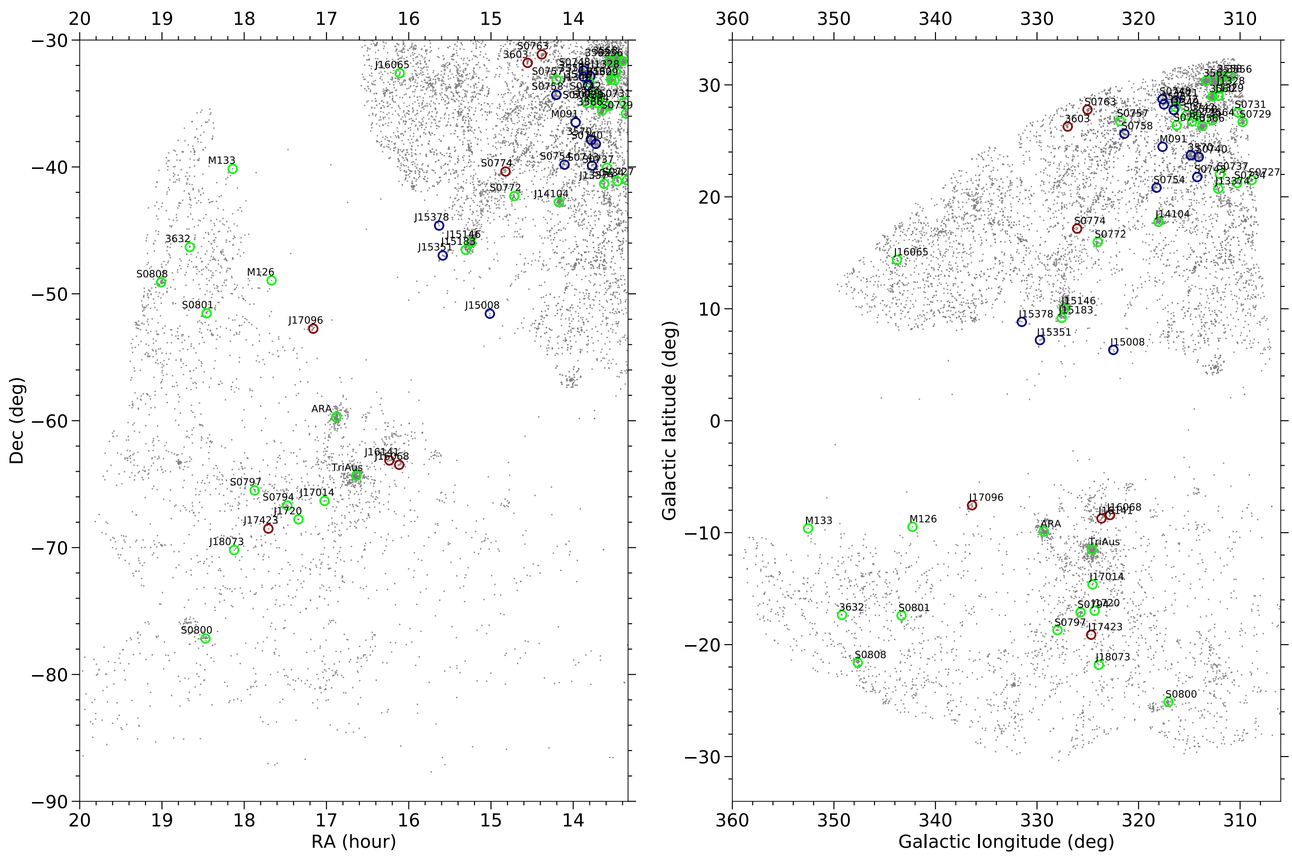

Fig. 10. TriAus and Shapley regions represented in RA, Dec (*left*), and in l,b coordinates (*right*) with the plane of the Milky Way crossing the figure. The positions of the discussed clusters in Tables 2 and 3 are represented in blue, green, and red circles in the ranges of $8000 \leq v < 12\,000$ km s^{-1}, $12\,000 \leq v < 18\,000$ km s^{-1}, and $18\,000 \leq v < 20\,000$ km s^{-1}, respectively.

clusters confirms the extension of the network in which the SSC is embedded, as suggested by these authors. The location of this set of clusters is shown in their Fig. 9. However the string of clusters passes directly behind a region of extremely high extinction of the galactic disk.

We added galaxies from the NED database within a radius of 10° around the center of the TriAus and ARA clusters, with a total of 2328 galaxies including the above four clusters already identified by Radburn-Smith et al. (2006), Kocevski & Ebeling (2006). The velocity histogram in Fig. 5

Table 3. Selection of 15 galaxy clusters from the CLASSIX survey in the region around the Triangulum Australis cluster as shown in Fig. 9.

(1)	(2)	(3)	(4)	(5)	(6)
RXC J1449.1−4022*	AbellS0774	14 49 11.5	−40 22 59	18 587	15
RXC J1500.8−5134		15 00 50.2	−51 34 04	10 253	14
RXC J1514.6−4558*	CIZA J1514.6−4558	15 14 36.3	−45 58 53	17 388	13
RXC J1518.3−4632*	CIZA J1518.3−4632	15 18 22.8	−46 32 25	16 679	12
RXC J1535.1−4658*	CIZA J1535.1−4658	15 35 09.1	−46 58 45	10 793	11
RXC J1537.8−4436		15 37 48.0	−44 37 18	11 512	10
RXC J1606.5−3246		16 06 35.5	−32 46 42	12 952	9
RXC J1606.8−6328		16 06 53.5	−63 28 36	18 408	8
RXC J1614.1−6307*	CIZA J1614.1−6307	16 14 07.9	−63 07 50	18 587	7
RXC J1638.2−6420*	TriAus cluster	16 38 21.8	−64 21 30	14 992	1
RXC J1653.0-5943*	Ara cluster	16 53 00.1	−59 43 08	14 390	2
RXC J1701.4−6619		17 01 26.1	−66 19 32	13 311	5
RXC J1709.6−5244		17 09 38.5	−52 44 49	19 127	6
RXC J1742.3−6830		17 42 24.0	−68 30 23	19 187	4
RXC J1807.3−7012	PKS 1801−702	18 07 23.5	−70 12 01	12 052	3

Notes. Asterisks refer to clusters already listed in Table 3 and numbers in the last column refer to the numbers in Fig. 9. The coordinates give the X-ray maximum, which may be different from the optical center quoted in Table 3.

of Radburn-Smith et al. (2006) shows the four rich clusters at $z \simeq 0.05$, which correspond to the recessional velocity histogram shown here (Fig. 7) centered at $\overline{V} = 15\,077$ km s^{-1}, with a dispersion of $\sigma = 3355 \pm 51$ km s^{-1}.

To study the interactions of the above wide TriAus region with the SSC, we extracted from the NED database all galaxies with velocities between $V = 8000$ and $V = 20\,000$ km s^{-1} to cover a wide region ranging ranging between RA = 12h30m and 20h00m and from Dec = −30° to Dec = −90° (J2000). We added the SSC velocity catalogue (Quintana et al. 2020) in the same velocity range and we finally obtained a set of 13 152 galaxies in this region, after eliminating duplicate objects.

Figure 8 shows the wedge diagrams from RA = 12h30 to RA = 18h and from Dec = −30° to Dec = −90° for these 13 152 galaxies. Many clusters are clearly visible, particularly in the region of the SSC and also around the TriAus centre. Several very elongated structures are strongly affected by extinction from the galactic plane.

In order to identify the already known structures in this wide area, we selected 50 identified clusters of galaxies from the NED database in the wide region ranging from RA = 13h20m to 20h00m and from Dec = −30° to Dec = −90° (J2000), including the SSC and TriAus, and with velocities ranging between 8000 and 20 000 km s^{-1}, which are listed in Table 2: (1) cluster name, (2) alternative name, (3) right ascension (J2000), (4) declination (J2000), (5) average heliocentric radial velocity in km s^{-1}.

If the TriAus and Ara clusters and several others could form a massive supercluster, they could influence the direction leading to the CMB Dipole. We have also looked into the studied region for ROSAT clusters and 2MASS galaxies in the same velocity range. We found 15 X-ray luminous clusters, which are listed in Table 3. In Fig. 9, we show the position of these clusters as well as galaxies from the 2MASS redshift survey. We note that seven clusters marked with an asterisk are also given in Table 2. Inside the two blue lines, the galactic HI column density is higher than 2.5×10^{21} cm^{-2}, namely, the region with high galactic absorption in X-rays but also high extinction in the optical. Thus, we cannot clearly follow the filament across this ZoA, but it seems to continue and connect the two denser regions on both sides of the galactic equator, as shown below.

A clearer view of the relationship between the cluster structures present above and below the Milky Way disk is displayed in Fig. 10, which shows the same region in RA and Dec (left) and in l and b (right) coordinates with 11 096 galaxies, where the positions of the clusters from Tables 2 and 3 are represented, with the SSC centre near the top right-hand corner. Noting their spatial and velocity distribution (color-coded) in the SE quadrant from the SSC, there is a noticeable filament of clusters, starting with CIZA J1410.4−4246, AS0772, CIZA J1514.6−4558, and CIZA J1518.3−4632, on the north side of the Milky Way disk, in the velocity range 12 000 km s^{-1}–18 000 km s^{-1} (circles in green color). Both Figs. 10a and b strongly suggest that the northern part of the filament, or extension, is just facing the southern part, across the absorbing Milky Way disk. The structure on the south side of the disk includes (in addition to the TriAus and Ara clusters) other clusters such as RXC J1701.4−6619, AS0794, CGJ1720−67.8, AS0797, and RXC J1807.3−7012, all following a filament extending from RA 14h10 and Dec −40° to RA 18h30 and Dec −70°, or even extending to AS0800 and Dec = −80°.

6. Discussion

In this work, we show that the massive TriAus cluster has several cluster companions within the same general redshift range. It is natural to think this group of clusters as part of one supercluster, centered on the TriAus cluster, which dominates by mass this supercluster. We call this the TriAus Supercluster. Obviously, this supercluster could be larger, particularly towards its northern and western side, if some other massive cluster still remains hidden behind the galaxy disk. In any case, it seems likely that some less massive and less luminous X-ray clusters may be hidden from view in that region, which appears as a natural gap in the connection from both sides on the disk (as shown in Fig. 10). An inspection of Figs. 8 and 9 of Jones et al. (2009) shows the general large-scale structures around the SSC from the 2dF Survey, showing a continuation of the “SSC front eastern wall” to the east, at a velocity centered on 11 000–12 000 km s^{-1} in Dec = −30° to Dec = −40°, which is seen in our Fig. 10 as well. It also shows a wide filament in the slice from Dec = −40° to Dec = −60° pointing to the East in the redshift $z = 0.05$ range, which would be coincident with the north section of the filament already described and with a narrow extension below the galactic plane. In the region of the TriAus and Ara clusters, the Dec = −60° to Dec = −90° slice shows a somewhat dispersed wide galaxy concentration. This is consistent with what we found in this search, including a few clusters up to a redshift of $z = 0.06$ (the ZoA is obviously empty).

These massive structures, namely, the SSC and TriAus supercluster, along with the connections between them, are hidden away behind the Great Attractor main source masses, located between radial recessional velocities 2000 km s^{-1} and 6000 km s^{-1} (already described in Radburn-Smith et al. 2006). Nevertheless, the important mass of the TriAus cluster (and its associated supercluster) will have some (possibly much smaller) effect in perturbing the galaxy velocity flows further away from the Great Attractor and beyond a radial velocity of 20 000 km s^{-1}. Therefore, their presence should be taken into account when calculating distant galaxy flows and the influence on the direction of the microwave dipole. However, the structures that are still hidden can further contribute to these effects if they do indeed exert a significant influence as well.

Acknowledgements. D.P. thanks the Instituto de Astrofísica of the Universidad Catolica for its hospitality at Santiago (Chile). H.B. thanks the Deutsche Forschungsgemeinschaft for support through the Excellence Cluster "Origins".

References

Ajello, M., Rebusco, P., Cappelluti, N., et al. 2009, ApJ, 690, 337
Andreuzzi, G., Bardelli, S., Scaramella, R., & Zucca, E. 1995, A&A, 337, 17
Arnaud, M., Pointecouteau, E., & Pratt, G. W. 2005, A&A, 441, 893
Ayral, B., & Saurer, W. 2005, MNRAS, 360, 125
Biviano, A., Murante, G., Borgani, S., et al. 2006, AA, 456, 23
Böhringer, H., Chon, G., Collins, C. A., et al. 2013, A&A, 555, A30
Böhringer, H., Chon, G., & Kronberg, P. P. 2016, A&A, 596, A22
Böhringer, H., Chon, G., Retzlaff, J., et al. 2017, AJ, 153, 220
Booth, R. S., De Block, W. J. G., Jonas, J. L., & Fanaroff, B. 2009, ArXiv e-prints [arXiv:0910.2935]
Bowen, I. S., & Vaughan, A. H. 1973, Appl. Opt., 12, 1430
Chow-Martinez, M., Andernach, H., Caretta, C. A., & Trejo-Alonso, J. J. 2014, MNRAS, 445, 4073
Cypriano, E. S., Lima Neto, G. B., Sodré, L., Jr, Kneib, J. P., & Campusano, L. E. 2005, ApJ, 630, 38
Davis, D. S., Bird, C. M., & Mushotzky, R. F. 1995, ApJ, 440, 48
Diaferio, A., Kauffmann, G., Balogh, M. L., et al. 2001, MNRAS, 323, 999
Dressler, A., & Shectman, S. A. 1988, AJ, 95, 284
Finn, R. A., Zaritski, D., & McCarthy, D. W., Jr 2004, ApJ, 604, 141
Girardi, M., Giuricin, G., Mardirossian, F., Mezzetti, M., & Boschin, W. 1998, ApJ, 505, 74
Kocevski, D. D., & Ebeling, H. 2006, ApJ, 645, 1043
Jones, D. H., Read, M. A., Saunders, W., et al. 2009, MNRAS, 399, 683
Kim, D.-W., & Fabbiano, G. 2013, ApJ, 776, 116
Kocevski, D. D., Mullis, C. R., & Ebeling, H. 2004, ApJ, 608, 721
Kurtz, M. J., Mink, D. J., Wyatt, W. F., et al. 1991, ASP Conf. Ser., 25, 432
Le Fèvre, O., Crampton, D., Lilly, S. J., Hammer, F., & Tresse, L. 1995, ApJ, 455, 60
McHardy, I. M., Lawrence, A., Kye, J. P., & Pounds, K. A. 1981, MNRAS, 197, 893
Markevitch, M. L., Sarazin, C. L., & Irwin, J. A. 1996, ApJ, 472, L17
Mink, D. J., & Wyatt, W. F. 1995, in Astronomical Data Analysis Software and Systems IV, eds. R. A. Shaw, H. E. Payne, & J. J. E. Hayes (San Francisco: Astron. Soc. Pac), ASP Conf. Ser., 77, 496
Pickles, A. J. 1985, ApJS, 59, 33
Pickles, A. J. 1998, PASP, 110, 863
Pratt, G. W., Croston, J. H., Arnaud, M., et al. 2009, A&A, 498, 361
Proust, D., Quintana, H., Carrasco, E. R., et al. 2006, A&A, 447, 133
Quintana, H., Carrasco, E. R., & Reisenegger, A. 2000, AJ, 120, 511
Quintana, H., Proust, D., Hertling, G., et al. 2009, Astron. Nachr., 330, 924
Quintana, H., Proust, D., Dunner, R., Carrasco, E. R., & Reisenegger, A. 2020, A&A, 638, A27
Radburn-Smith, D. J., Lucey, J. R., Woudt, P. A., Kraan-Korteweg, R. C., & Watson, F. G. 2006, MNRAS, 369, 1131
Scaife, A. N. N., Oozeer, N., de Gasperin, F., et al. 2015, MNRAS, 451, 4021
Sereno, M., Lubini, M., & Jetzer, Ph 2010, AA, 518, 55
Shectman, S. A. 1989, Year Book 89 (Washington: Carnegie Inst.), 25
Solovyeva, L., Anokhin, S., Feretti, L., et al. 2008, A&A, 484, 621
Tonry, J., & Davis, M. 1979, AJ, 84, 1511
Trümper, J. 1993, Science, 260, 1769
Woudt, P. A., Kraan-Korteweg, R. C., & Fairall, A. P. 1999, A&A, 352, 39

Appendix A: Additional table

Table A.1. The new heliocentric radial recessional velocities catalogue in TriAus and AS794. Each column is described in Sect. 3.

(1)	(2)	(3)	(4)	(5)	(6)	(7)
C101 (TriAus)						
1	16 31 27.82	-64 24 44.4	14795	55	5.12	
2	16 31 29.66	-65 24 46.7	11942	62	5.84	em : OII
3	16 32 19.16	-64 54 29.6	15010	59	6.07	em : OII
4	16 32 20.52	-64 31 44.3	14863	59	4.76	
5	16 32 26.80	-64 47 25.8	4350	66	3.47	em: Hβ,Hα
6	16 32 42.25	-64 49 59.2	4419	37	8.08	
7	16 33 00.74	-64 29 32.4	4477	56	4.12	
8	16 33 08.21	-64 19 44.6	14907	39	6.09	
9	16 33 20.17	-64 22 45.3	14908	40	8.26	
10	16 34 21.62	-65 21 29.2	15398	54	6.03	
11	16 34 56.04	-65 07 58.2	16930	36	8.08	
12	16 35 00.55	-65 30 27.7	15587	73	4.72	
13	16 35 02.67	-64 50 49.8	11518	33	8.33	
14	16 35 20.38	-65 28 29.8	15214	47	5.78	
15	16 35 26.45	-64 37 27.8	13970	86	2.54	very weak
16	16 35 31.75	-64 55 01.5	12807	53	5.93	
17	16 35 48.48	-64 36 02.0	13363	59	4.86	
18	16 35 52.47	-64 20 39.8	14666	56	5.29	
19	16 35 53.17	-64 22 00.5	13856	57	4.44	
20	16 36 20.36	-65 31 46.6	2908	30	8.16	em: OII,2OIII
21	16 36 22.77	-65 36 49.3	9655	84	4.28	
22	16 36 28.65	-65 33 09.9	12514	122	2.78	very weak
23	16 36 30.30	-64 26 01.5	11954	52	5.83	
24	16 36 32.81	-64 48 42.3	13847	54	4.32	
25	16 36 41.05	-64 26 04.8	11877	64	3.31	weak
26	16 37 06.31	-64 28 53.3	12640	22	12.23	em: OII,Hβ,2OIII
27	16 37 13.95	-64 22 02.8	13173	48	7.93	
28	16 37 15.23	-64 20 04.2	15408	41	6.69	
29	16 37 29.67	-64 34 22.5	14104	38	7.72	
30	16 37 52.54	-64 48 47.7	4599	38	8.08	
31	16 38 00.93	-64 29 38.2	15214	96	4.01	
32	16 38 02.05	-64 18 60.0	15323	54	8.24	
33	16 38 05.18	-64 19 50.8	16659	50	5.55	
34	16 38 18.00	-64 21 36.8	14801	54	4.89	
35	16 38 26.41	-64 25 28.6	15514	36	9.75	
36	16 38 29.47	-64 18 15.6	15497	40	7.77	
37	16 38 32.88	-64 23 54.2	15524	73	3.17	weak
38	16 38 35.41	-64 41 31.2	14319	58	7.00	
39	16 38 40.27	-64 36 08.0	15360	40	7.56	
40	16 38 48.03	-64 20 03.9	14547	52	5.50	
41	16 38 50.79	-65 07 39.1	14633	41	6.46	
42	16 38 51.35	-64 26 26.8	12251	94	3.77	
43	16 38 53.72	-64 22 25.9	17769	37	8.06	
44	16 38 57.79	-64 23 59.6	13820	54	5.49	
45	16 38 58.43	-64 21 06.1	16008	48	4.42	
46	16 39 02.59	-65 05 05.6	14689	44	8.32	
47	16 39 07.86	-64 28 48.1	15229	51	6.73	
48	16 39 08.11	-64 30 37.1	15032	34	9.41	
49	16 39 11.31	-64 36 00.3	14906	49	5.58	
50	16 39 15.17	-64 24 22.0	17607	48	6.10	
51	16 39 18.26	-64 22 39.4	15713	48	5.11	
52	16 39 21.61	-65 15 44.8	14535	61	6.41	
53	16 39 28.27	-64 29 03.1	13298	45	6.80	
54	16 39 35.25	-64 19 59.3	16451	98	3.31	
55	16 39 52.23	-64 48 55.8	14393	40	8.70	
56	16 39 57.70	-64 33 28.0	15646	34	8.86	
57	16 39 58.15	-64 26 27.9	15901	54	6.73	
58	16 39 58.84	-65 07 33.4	13199	64	5.06	
59	16 40 09.50	-64 29 17.5	16002	42	6.91	
60	16 40 11.24	-64 23 12.1	12579	99	2.74	weak
61	16 40 13.44	-65 12 19.8	15260	62	4.85	
62	16 40 20.93	-64 26 11.1	14459	47	5.60	
63	16 40 33.42	-64 22 56.6	15689	53	6.12	
64	16 41 08.07	-64 41 30.5	13547	48	5.14	
65	16 41 49.65	-65 09 51.3	15203	77	4.98	
66	16 42 37.27	-64 40 16.5	13929	58	5.17	

Table A.1. continued.

(1)	(2)	(3)	(4)	(5)	(6)	(7)
67	16 42 38.00	-65 39 43.3	11696	30	11.44	
68	16 42 42.19	-64 52 43.3	13997	27	10.80	
69	16 42 45.36	-64 50 28.2	14256	30	9.17	em : OII
70	16 42 50.48	-64 58 33.0	14832	54	3.52	
71	16 43 31.12	-64 48 17.3	14516	47	7.65	
72	16 43 49.32	-64 58 55.4	15243	52	6.96	
73	16 43 55.06	-65 28 48.5	14639	48	6.70	
74	16 44 09.29	-64 54 40.7	14920	41	8.82	
75	16 44 14.57	-64 57 28.9	14912	75	4.48	
76	16 44 46.18	-65 06 31.4	15267	49	6.30	
AS0794						
1	17 20 59.12	-66 30 23.9	37325	54	3.29	
2	17 21 12.00	-66 14 06.4	36962	51	4.27	
3	17 21 33.00	-66 04 37.8	12991	42	7.43	
4	17 21 56.40	-66 56 43.2	33951	73	4.68	
5	17 21 59.05	-65 51 21.4	14662	34	8.10	
6	17 23 13.27	-66 23 18.2	17092	73	4.05	
7	17 23 24.71	-66 43 50.3	12470	78	2.77	weak
8	17 23 34.69	-66 28 56.6	17204	38	5.80	em: OII,Hβ,2OIII
9	17 23 54.82	-67 06 12.7	18549	48	4.68	em: OII,Hβ,2OIII
10	17 24 23.53	-66 06 57.9	37244	54	5.92	
11	17 24 30.48	-66 28 24.0	12616	32	8.89	
12	17 25 03.76	-65 58 37.8	8334	60	4.11	
13	17 25 14.77	-66 03 59.9	12775	30	9.21	
14	17 25 16.47	-65 55 45.1	12208	43	5.37	
15	17 25 22.25	-67 11 57.1	42006	55	3.70	
16	17 25 34.06	-67 09 10.7	16319	46	6.29	
17	17 25 54.03	-66 33 13.9	13306	76	3.14	
18	17 25 54.72	-65 56 01.1	15832	52	4.92	
19	17 26 27.18	-66 32 31.3	12549	78	2.93	weak
20	17 26 39.56	-65 51 56.5	11248	58	2.82	weak
21	17 27 00.94	-66 35 45.1	12137	58	3.24	
22	17 27 07.93	-66 38 23.6	12606	49	6.34	
23	17 27 23.36	-65 58 39.1	5554	72	5.45	em: OII,Hβ,2OIII
24	17 27 33.22	-67 14 41.6	22606	57	3.52	
25	17 27 33.29	-66 07 26.0	6461	44	6.20	
26	17 27 37.32	-66 45 55.9	12684	38	8.39	
27	17 28 01.83	-66 47 02.0	11795	61	4.26	
28	17 28 13.21	-66 51 50.8	12888	30	12.06	
29	17 28 14.90	-66 40 15.4	13478	86	3.68	
30	17 28 25.40	-66 28 35.5	12983	72	3.48	weak
31	17 28 40.97	-66 40 54.3	13135	40	7.54	
32	17 28 43.02	-66 28 34.9	12759	74	3.32	
33	17 28 43.78	-65 57 28.9	22637	45	5.31	em : em: Hβ,2OIII
34	17 28 56.14	-66 09 01.0	6522	49	5.56	
35	17 28 59.06	-66 47 45.3	12391	41	6.75	
36	17 29 06.68	-66 42 29.0	13127	45	6.97	
37	17 29 28.15	-66 34 32.7	12633	44	6.65	
38	17 29 33.78	-66 51 39.6	13020	71	3.23	weak
39	17 29 46.37	-66 42 53.5	12140	51	3.71	
40	17 29 55.25	-66 44 27.3	13095	51	5.89	
41	17 30 13.18	-66 28 14.9	13055	77	2.57	very weak
42	17 30 28.66	-66 31 54.1	14773	57	4.16	
43	17 30 39.70	-65 58 43.2	14463	29	9.82	
44	17 30 45.46	-66 33 34.5	12857	38	8.15	
45	17 30 53.18	-66 47 12.3	12717	24	12.36	
46	17 31 02.32	-65 57 38.1	44600	52	3.49	
47	17 32 16.62	-66 33 37.5	12943	47	6.13	
48	17 32 16.71	-66 33 37.5	12943	47	6.13	
49	17 32 23.96	-66 51 40.1	18748	64	3.90	
50	17 33 01.27	-66 46 38.0	12199	31	10.04	
51	17 33 01.53	-66 55 55.7	12708	77	2.51	very weak
52	17 34 03.25	-67 17 23.9	21792	64	3.50	weak
53	17 34 10.02	-66 39 13.1	12557	48	7.64	
54	17 35 21.07	-67 09 36.0	18548	44	6.45	
55	17 35 33.84	-67 04 19.3	18516	45	6.57	